INTERNATIONAL JOURNAL FOR NUMERICAL METHODS IN FLUIDS
Int. J. Numer. Meth. Fluids 2012; **69**:1363–1376
Published online 15 July 2011 in Wiley Online Library (wileyonlinelibrary.com/journal/nmf). DOI: 10.1002/fld.2644

A novel peristaltic micropump with low compression ratios

Yeng-Yung Tsui*,† and Tso-Chang Chang

Department of Mechanical Engineering, National Chiao Tung University, Hsinchu 300, Taiwan

SUMMARY

It is common for peristaltic micropumps to have large compression ratios. In the limit, the chamber of the pump is completely blocked by the membrane to prevent back flow. Different from this kind of pump, a micropump with small compression ratios is proposed in this study. With small oscillation amplitudes the membrane of the pump can reciprocate at high frequencies to improve its pumping flow. Both the multidimensional method and the lumped-element method are employed for analysis. For this kind of peristaltic micropump the working fluid is allowed to flow freely in the forward and backward directions. Therefore, the operating sequences for the high-compression ratio type of pumps are not appropriate. It is shown that the theoretical net flow rate is zero for the four-phase and six-phase modes of sequence and becomes negative for the three-phase mode unless regulators, such as the nozzle/diffusers, are incorporated to rectify the flow. However, this pump becomes very attractive by reversing the operating sequence of the three-phase mode because positive net flow is yielded. It is seen that with the reversed three-phase mode and the nozzle/diffuser as connecting channels, the pumping effectiveness is greatly enhanced. The pumps with both two chambers and three chambers are under consideration in the study. Copyright © 2011 John Wiley & Sons, Ltd.

Received 26 March 2010; Revised 2 June 2011; Accepted 3 June 2011

KEY WORDS: peristaltic micropump; low compression ratio; lumped-system analysis; CFD simulation

1. INTRODUCTION

A variety of principles have been proposed to operate micropumps. The most common one is the use of piston-like reciprocating membrane, which oscillates in a periodic manner to do work on the working fluid. A classic way to regulate the flow direction in the pump is to install microvalves at the inlet/outlet of the pump chamber. Microvalves can be operated in either active or passive ways [1]. The small scales of the valves together with their complicated structure make fabrication rather difficult. The periodic open and close of these valves sometimes lead to mechanical wear and fatigue. In addition, there is a risk of valve blockade caused by small particles embedded in the fluid.

To avoid the above problems, the concept of so called valveless micropumps emerges. Instead of moving valves, conduits with different impedances for different flow directions are incorporated. Because the flow resistance is lower in a favorable direction than in the other direction, there results a net flow in this direction when the fluid is pumped into and out of the pump chamber through these conduits periodically by the reciprocating membrane. Realization of such flow regulators in micropumps includes nozzle/diffuser type channels [2, 3], valvular conduits of Tesla [4], and vortex diodes [5].

Another kind of micropump is based on the concept of peristalsis. Peristaltic transport in flexible tubes is generated by a progressive wave of area contraction/expansion propagating down the wall of the tube containing fluid, which can be found in many biological systems, such as vasomotion of

*Correspondence to: Yeng-Yung Tsui, Department of Mechanical Engineering, National Chiao Tung University, Hsinchu 300, Taiwan.
†E-mail: yytsui@mail.nctu.edu.tw

arterioles and venules, flow of urine from kidney to bladder, and the transport of lymph in the lymphatic vessels, among others. To understand the mechanism responsible for the peristaltic transport, Shapiro *et al*. [6] obtained analytic solutions for two-dimensional flexible tube flows by assuming that the Reynolds number is small enough to neglect the flow inertia and that the wave length is very long compared with the width of the tube. The analysis of Fung and Yih [7] was based on small perturbation theory, which is valid for a small ratio of wave amplitude to tube width. In contrast to that of Shapiro *et al*., the effect of the nonlinear convective acceleration was included.

In microfluidic systems, peristalsis can be realized via employing a number of pumping stages. The first peristaltic micropump was presented by Smits [8], which had three pump chambers linked in a series by etched channels. The opening or closing of each chamber is driven by a piezoelectric disk at 120° out of phase with one another to simulate the oscillating motion of the flexible wall of the peristaltic tube. In later studies, various actuators and different fabrication processes were reported. Cao *et al*. [9] proposed a pump actuated by bulk PZT (piezoelectric transducer) disks, to be used in medical drug delivery systems. Bu *et al*. [10] and Husband *et al*. [11] integrated a piezoelectrically driven micropump into a chip for polymerase chain reaction. Xie *et al*. [12] reported an electrostatically actuated micropump, being entirely surface micromachined using a multilayer parylene technology. The micropump presented by Jeong *et al*. [13] adopted the thermopneumatic actuation and was fabricated using multistacked polydimethylsiloxane (PDMS) molding technique. Goulpeau *et al*. [14] also employed the PDMS multilayer technology for fabrication. The pump is operated with a pneumatic system. In the above studies, the pumps consist of three chambers. Berg *et al*. [15] showed that peristalsis can be realized with two chambers. Their pumps were also fabricated with use of PDMS and activated pneumatically.

According to the actuation sequence, the three-chamber peristaltic pump can be operated in different modes: six-phase, four-phase and three-phase. In six-phase mode, only one membrane is actuated to open or close one of the chambers in each phase, whereas two membranes are involved in three-phase sequence. All the three modes were considered in the study of Jang and Yu [16]. It was shown by them that the four-phase sequence has the best performance in terms of net flow rate. The two-chamber micropump of Berg *et al*. [15] was operated in three-phase and four-phase modes. Their results reveal that the four-phase mode can lead to net flow rate comparable to the three-chamber micropump in three-phase mode.

To analyze the flow behavior of the peristaltic micropump and to evaluate a pump design quickly, lumped-element methods have been employed. In the simple lump model used by Na *et al*. [17], the pump is assumed to be working in a steady state and the head loss of the flow through each element of the pumping system is taken into account in the Bernoulli equation [18]. The dynamics of the pumping process was included in the model of Goldschmidtboing *et al*. [19], which is based on the analogy of the fluidic system to the electric network. Lin and coworkers [12, 20] reported a dynamic simulation of an electrostatically actuated peristaltic micropump involving coupled fluid flow and structural motion. The membrane motion is represented by an effective spring subjected to hydrodynamic and electrostatic forces. The hydrodynamic forces are obtained from lubrication theory [21].

In general, the working principle for peristaltic micropumps, as seen in the given studies above, is applicable to the condition of large compression ratio, which is defined as the stroke volume swept by the membrane to the dead volume of the pump chamber. In the limit of high compression ratio, the flow in the chamber is obstructed by the moving membrane completely. Thus, the movement of the membrane functions not only to drive the fluid to flow, but also to work as an active valve to prevent back flow. A sketch of the working process for the three operating modes of the three-chamber micropump is shown in Figure 1. The three-phase and four-phase modes of the two-chamber pump of Berg *et al*. [15] operate in the same sequences as the corresponding modes for the three-stage one except that the third chamber is truncated.

In some designs, the pumps operate at high frequencies, but with small membrane deflections [2, 3]. With these designs adopted in peristaltic pumps, as considered in the present study, the working fluid is allowed to flow freely in both directions in the channels connecting the individual pump chambers and the inlet and outlet. Therefore, the above working principle becomes questionable. It needs to be mentioned that in many applications, such as the drug delivery system, particles are

DOI: 10.1002/fld

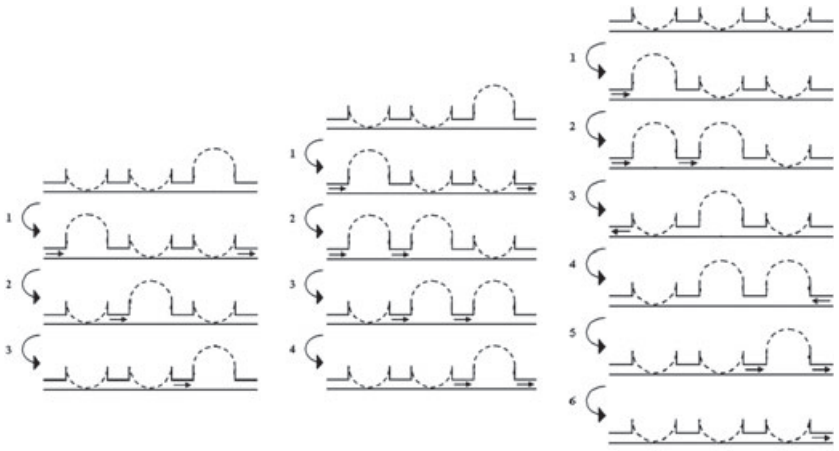

(a) 3-phase (b) 4-phase (c) 6-phase

Figure 1. Illustration of the peristaltic sequence for the high-compression ratio three-chamber micropump. By truncating the last chamber in (a) and (b), it reduces to the three-phase and four-phase sequences for the two-chamber micropump.

contained in the working fluid. This low-compression ratio peristaltic micropump is particularly attractive for these applications because of its little chance to cause clog.

The development of CFD by solving Navier–Stokes equations has become mature and made it a useful analytical tool. Application of this multidimensional technique to study the flow in valveless micropumps has been realized by Tsui and Lu [22] and Ha *et al*. [23]. It was shown that reasonably good agreement was obtained in comparison with experiments. Although this approach can provide accurate solutions and detailed flow field, it requires large computer resources and is very time consuming. An alternative and much simple approach is the lumped-element method, which provides fast solutions for bulk properties of the flow system and is suitable in the preliminary design stage. As seen from the literature survey given above, it was mainly this method used for analysis in the studies of peristaltic micropumps. In the past several years, a multidimensional solution procedure, together with a lumped-element method, was developed by the group of the present authors and has given good results [22, 24]. To the best of our knowledge, the investigation of the flow characteristics of low-compression ratio peristaltic micropumps has not been revealed in the literature. The aim of the present study is to fulfill this task using the above two analytical approaches.

2. MATHEMATICAL MODELS

2.1. Multidimensional method

The flow in the micropump is assumed to be laminar and incompressible because of its microscale and the low flow velocity. Its dynamics is governed by the conservation equations for the mass and momentum.

$$\nabla \bullet \vec{V} = 0 \tag{1}$$

$$\frac{\partial \rho \vec{V}}{\partial t} + \nabla \bullet \left(\rho \vec{V} \vec{V} \right) = -\nabla P + \mu \nabla^2 \vec{V} \tag{2}$$

where ρ is the density, $\vec{V}$ the velocity vector, P the pressure and μ the viscosity of the working fluid.

The finite volume method is employed such that the conservation law is maintained during discretization. The geometry of the flow field in the pump is inevitably complicated. To cope with the

DOI: 10.1002/fld

irregular geometry, computational grids are constructed in the unstructured manner. The transport equations are integrated over a control volume, followed by applying the divergence theorem to transform the transport terms, that is the convection and diffusion terms, into surface integrals.

$$\int_{CV} \frac{\partial \rho \phi}{\partial t} \mathrm{d}v + \int_{CS} (\rho \vec{V} \phi) \bullet \mathrm{d}\vec{s} = \int_{CS} \mu \nabla \phi \bullet \mathrm{d}\vec{s} + \int_{CV} S_\phi \mathrm{d}v \tag{3}$$

where ϕ represents the velocity component and S_ϕ the corresponding pressure gradient. The convective flux through each face of the control volume surface is represented by

$$F_\mathrm{f}^c = \left(\rho \vec{V} \bullet \vec{s}\right)_\mathrm{f} \phi_\mathrm{f} = \dot{m}_\mathrm{f} \phi_\mathrm{f} \tag{4}$$

where the subscript f denotes the considered face, $\vec{s}_\mathrm{f}$ is the surface vector of the face (see Figure 2), $\dot{m}_\mathrm{f}$ the mass flux through the face. The value ϕ_f transported by the convection at the face is calculated by blending the upwind (UD) and central (CD) differencing schemes.

$$F_\mathrm{f}^c = F^{\mathrm{UD}} + \gamma \left(F^{\mathrm{CD}} - F^{\mathrm{UD}}\right) \tag{5}$$

where

$$F^{\mathrm{UD}} = \max(\dot{m}_\mathrm{f}, 0)\phi_\mathrm{P} + \max(-\dot{m}_\mathrm{f}, 0)\phi_\mathrm{C} \tag{6a}$$

$$F^{\mathrm{CD}} = \dot{m}_\mathrm{f}[(1-w)\phi_\mathrm{P} + w\phi_\mathrm{C}] \tag{6b}$$

In the CD, w represents a factor for the interpolation between the two centroids P and C on the two sides adjacent to the face f (Figure 2). The coefficient γ is a weighting factor between the UD and the CD. A value of 0.9 is chosen such that the scheme is biased towards the second-order accurate CD. The diffusive flux through a face is approximated by

$$F_\mathrm{f}^d = \frac{\mu s_\mathrm{f}^2}{\vec{\delta}_{\mathrm{PC}} \bullet \vec{s}_\mathrm{f}} (\phi_\mathrm{C} - \phi_\mathrm{P}) + \mu \overline{\nabla \phi}_\mathrm{f} \bullet \left(\vec{s}_\mathrm{f} - \frac{s_\mathrm{f}^2}{\vec{\delta}_{\mathrm{PC}} \bullet \vec{s}_\mathrm{f}} \vec{\delta}_{\mathrm{PC}}\right) \tag{7}$$

where $\vec{\delta}_{\mathrm{PC}}$ is the vector connecting the nodes P and C (Figure 2) and $\overline{\nabla \phi}_\mathrm{f}$ is the gradient at the face obtained by linear interpolation from the gradients at the two nodes.

For the calculation of incompressible flow it is essential to deal with the coupling between the momentum and continuity equations. A common approach to tackle this issue is the use of the Semi-Implicit Method for Pressure-Linked Equations (SIMPLE) algorithm [25]. However, this method requires iteration among the momentum equation and the pressure-correction equation, which is very time-consuming. Therefore, the noniterative Pressure Implicit with Splitting of Operators (PISO) algorithm [26] is adopted in this study. This method is briefly described in the following.

By using the pressure field obtained in the last time step, velocities can be obtained by solving the corresponding momentum equations sequentially. The resulting velocity field is then corrected

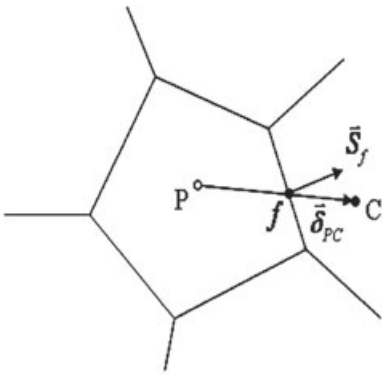

Figure 2. Illustration of a control volume with neighboring cells.

DOI: 10.1002/fld

by updating the pressure in such a way that the mass is conserved in each control volume. In this correction step, a linear relationship is assumed between the pressure correction and the velocity correction. By forcing the corrected velocities to satisfy the continuity constraint, a pressure-correction equation is obtained. Details about this derivation can be found in the study of Tsui and Pan [27]. A second corrector is entailed in the solution procedure in order to make the pressure field further get rid of the mass residual left in the last correction step and to yield better approximation to the conservation of momentum. In this second correction step, the contribution to the momentum equation from neighboring nodes is retained. The resulting pressure-correction equation is similar to that of the first corrector, but with a different source term. More similar correctors can be imposed. However, only two correction steps are employed because the accuracy of the solution is within the temporal truncation error after these steps.

A sketch of the considered micropump is shown in Figure 3. The pump consists of three main chambers together with two small chambers functioning as inlet and outlet. For the two-chamber pump the last chamber is excluded. The chambers are connected by channels of the nozzle/diffuser type or straight duct. The dimensions of the chambers and channels are shown in the figure. A PZT disk is attached to each membrane on top of the main chambers. The oscillating movement of the membrane is activated by the PZT disk.

It was shown by Tsui and Lu [22] that good agreement with experiments can be obtained with an assumption of a simple curved surface for the deflection of the membrane. In the following, the displacement of each membrane is assumed to be of the trapezoidal profile, oscillating in a simple harmonic motion.

$$Z(r,t) = -h_{\max} \min\left[1, \frac{r_0 - r}{r_0 - r_1}\right] \cos(2\pi f t) \tag{8}$$

where r_0 is the radius of the chamber, r_1 that of the PZT disk, $h_{\max}$ the amplitude of oscillation at the center of the membrane, and f the frequency. Compared with the chamber height of 0.2 mm, the deflection of the membrane ($h_{\max} = 1\,\mu$m) is so small that its effect on the variation of the chamber volume can be ignored. The compression ratio, defined as the ratio of the volume swept by the oscillating membrane to the dead volume of the chamber, is 0.0076 for the present pump configuration. Therefore, instead of the moving boundary, the membrane is fixed at its neutral position. A velocity condition, derived from the above equation, is imposed on this fixed boundary.

$$V(r,t) = 2\pi f h_{\max} \min\left[1, \frac{r_0 - r}{r_0 - r_1}\right] \sin(2\pi f t) \tag{9}$$

A zero pressure is set at the inlet of the pump and a specified back pressure is prescribed at the outlet. With the given pressures, the mass flow rates through these open boundaries need to be determined. A method, suitable for the noniterative algorithm given in the above, has been developed. First, the boundary pressure is prescribed on the centroids of the cells next to the open boundaries.

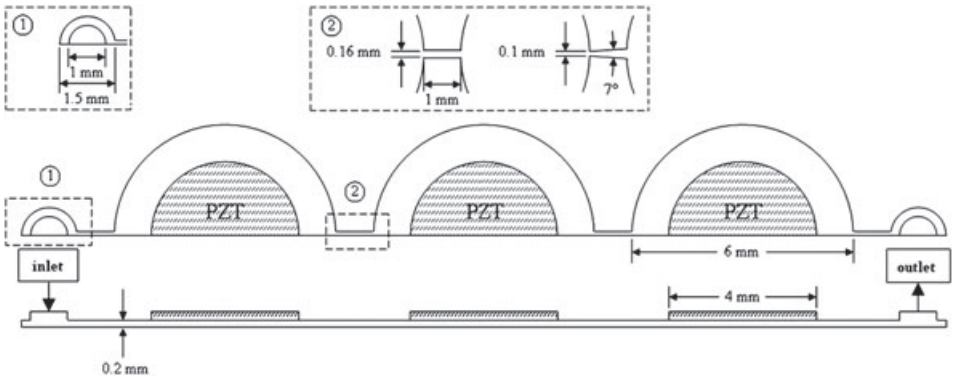

Figure 3. Configuration of the three-chamber micropump.

DOI: 10.1002/fld

Then, an extrapolation practice is made to find the pressures on the boundary faces. After the mass fluxes through the internal face of all control volumes are calculated using the boundary pressures by the solution method described above, the mass flux through the boundary face of each boundary cell can be obtained using the mass conservation principle. More details about this procedure can be found in [22].

In the simulation, water is employed as the working fluid with $\rho = 997$ kg/m^3 and $\mu = 8.5 \times 10^{-4}$ Ns/m^2. The piezo disk of the membrane for each chamber is actuated at a frequency of 2200 Hz. Each oscillating period of the membrane is divided into 600 time steps, which is equivalent to 7.57×10^{-7} s for each time step. Calculations start with a stagnant state initially and end after five peristaltic periods. It was found that after a transient stage of three periods the flow becomes periodically steady.

2.2. *Lumped-system analysis*

A simple method, based on the concept of lumped elements [24], is also employed for analysis. In this method, the head loss across the pump from the inlet to the outlet is assumed to be mainly caused in the channels connecting the individual chambers and the inlet and outlet. The losses in the chambers can be neglected because of the small compression of the pump. The fluid system can then be represented by an electrically equivalent circuit with the flow rate analogous to the electric current and the pressure to the voltage. For the nozzle/diffuser as the connecting channel, the pressure difference ΔP across this element is related to the volumetric flow rate Q through it as in a R-L circuit

$$\Delta P = RQ + L\frac{\mathrm{d}Q}{\mathrm{d}t} \tag{10}$$

Here, R represents flow resistance.

$$R = \left[\max\left(\frac{Q}{|Q|}, 0\right)k_\mathrm{d} - \min\left(\frac{Q}{|Q|}, 0\right)k_\mathrm{n}\right]\frac{\rho}{2A_t^2}|Q| \tag{11}$$

where k_d and k_n are the loss coefficients corresponding to the diffuser and nozzle functions, respectively, and A_t is the throat area. The loss coefficients are related to the Reynolds number, or the flow rate. The correlations given by Tsui and Lu [22] are employed because the same nozzle/diffuser elements are used in both studies. The flow inertia is represented by the inductance term with L defined by

$$L = \frac{2\rho\ell}{(A_\mathrm{t} + A_l)} \tag{12}$$

where ℓ is the length of the channel and A_l is the cross-sectional area at the larger side of the nozzle/diffuser element.

The equivalent electrical circuit for the three-chamber micropump is shown in Figure 4. With P_1, P_2, and P_3 as the pressures in the chambers and P_in, P_out as the pressures at inlet and outlet, the following relations are obtained:

$$P_\mathrm{in} - P_1 = R_\mathrm{in}Q_\mathrm{in} + L\frac{\mathrm{d}Q_\mathrm{in}}{\mathrm{d}t} \tag{13a}$$

$$P_1 - P_2 = R_\mathrm{c1}Q_\mathrm{c1} + L\frac{\mathrm{d}Q_\mathrm{c1}}{\mathrm{d}t} \tag{13b}$$

$$P_2 - P_3 = R_\mathrm{c2}Q_\mathrm{c2} + L\frac{\mathrm{d}Q_\mathrm{c2}}{\mathrm{d}t} \tag{13c}$$

$$P_3 - P_\mathrm{out} = R_\mathrm{out}Q_\mathrm{out} + L\frac{\mathrm{d}Q_\mathrm{out}}{\mathrm{d}t} \tag{13d}$$

DOI: 10.1002/fld

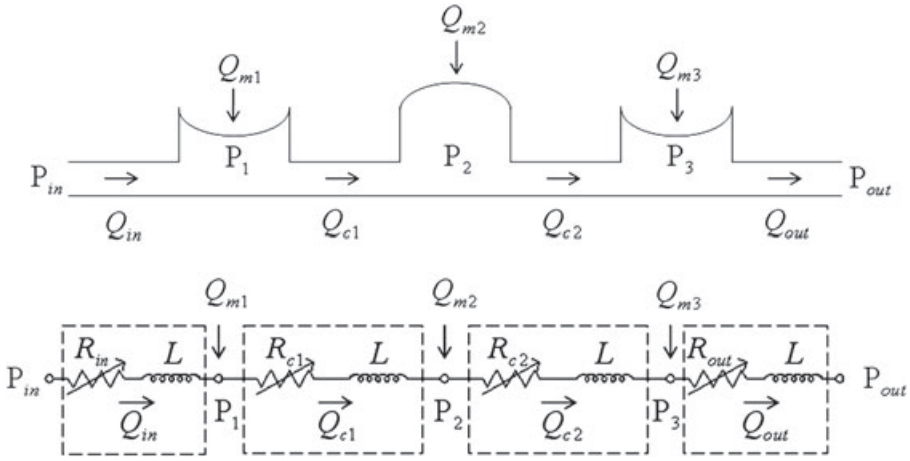

Figure 4. Illustration of the flow system of the three-chamber micropump and the equivalent electric circuit.

where Q_{in}, Q_{c1}, Q_{c2}, and Q_{out} are the volumetric fluxes through the four connecting channels. The mass conservation applied to the three chambers leads to the following equations:

$$Q_{\text{c1}} - Q_{\text{in}} = Q_{\text{m1}} \tag{14a}$$

$$Q_{\text{c2}} - Q_{\text{c1}} = Q_{\text{m2}} \tag{14b}$$

$$Q_{\text{out}} - Q_{\text{c2}} = Q_{\text{m3}} \tag{14c}$$

where Q_{m1}, Q_{m2}, and Q_{m3} represent the volumetric fluxes generated by the reciprocating membranes. Thus, there are seven equations in this model to be solved for the unknowns of three chamber pressures and four flow rates through the connecting channels. The differential equations given by (13a)–(13d) can be discretized by, say, the backward Euler scheme [28]. The resulting system of equations together with Equations (14a)–(14c) can then easily be solved using MATLAB software (MathWorks, Natick, MA, U.S.A.).

3. RESULTS AND DISCUSSION

The configuration of the micropump under consideration is presented in Figure 3. For the three-chamber pump, the operating sequences for the three-phase, four-phase, and six-phase modes are shown in Figure 5. The three-phase and four-phase modes for the two-chamber pump are identical to those shown in Figures 5(a) and (b) except that the third chamber is excluded. As an example, the flow fluxes resulting from the actuation of the membranes are given in the following for the three-phase mode:

$$Q_{\text{m1}} = \begin{cases} -\forall_{\max}\omega \sin \omega t & 0 < t < 2T/3 \\ 0 & 2T/3 < t < T \end{cases} \tag{15a}$$

$$Q_{\text{m2}} = \begin{cases} 0 & 0 < t < T/3 \\ \forall_{\max}\omega \sin \omega t & T/3 < t < T \end{cases} \tag{15b}$$

$$Q_{\text{m3}} = \begin{cases} \forall_{\max}\omega \sin \omega t & 0 < t < T/3 \\ 0 & T/3 < t < 2T/3 \\ -\forall_{\max}\omega \sin \omega t & 2T/3 < t < T \end{cases} \tag{15c}$$

where $\forall_{\max}$ is half of the volume swept by the membrane, $\omega (= 2\pi f)$ the angular speed of the membrane oscillation, f the oscillation frequency, and $T = 3/2f$ is the period of the peristalsis.

DOI: 10.1002/fld

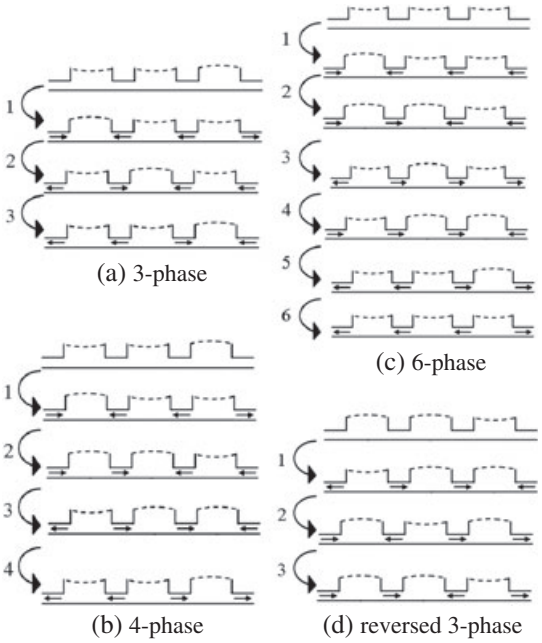

Figure 5. Illustration of the peristaltic sequence for the low-compression ratio three-chamber micropump. By truncating the last chamber in (a), (b), and (d), it reduces to the three-phase, four-phase, and reversed three-phase sequences for the two-chamber micropump.

It is noted that for an n-phase mode the period T is $n/2f$. Similar expressions for the other modes can be obtained according to the sequences shown in Figure 5.

Validation of the analytical methods described above has been made in the previous study [22] for the configuration with a single chamber. With a suitable assumed deflection profile for the membrane, good agreement with measurements was obtained. The same pump is employed in this study, but with multiple chambers operating in a peristaltic manner. To examine the grid sensitivity, five different meshes, including 118,332, 152,240, 192,808, 228,600, and 291,264 cells, were tested for the three-chamber micropump in the reversed three-phase mode, as shown in Figure 5(d), with zero back pressure. The net flow rates corresponding to the tested meshes are 1.49, 1.51, 1.43, 1.42, and 1.43 ml/min. It is obvious that the third level of mesh with 192,808 cells can lead to a grid independent solution, and is therefore used in the following computations. As for the two-chamber pump, the number of computational cells is 140,558.

A computational grid for the three-chamber pump, generated using the grid generation software GAMBIT (ANSYS, Inc., Canonsburg, PA, USA), is illustrated in Figure 6. Calculations were performed on a PC with Intel Pentium dual-core CPU E6500 (@ 2.93 GHz) (Intel Corp., Santa Clara, CA, USA) installed. The solution is advanced with a time step of 0.757 μs. A job of five-peristaltic period runs requires 4500 time steps and takes about 15 h of CPU time. Hence, around 12 s of CPU time is needed for a computational time step.

To illustrate the flow field, pressure contours, and streamlines at t = T/6, T/2, and 5T/6, corresponding to the first, second, and third stage of the reversed three-phase mode, are presented in Figure 7. As seen in Figure 5(d), Chamber 1 on the left is in the pump mode (i.e., compressed) while Chamber 3 on the right is in the supply mode (i.e., expanded) in the first phase. As a consequence, the pressure is high in the former and low in the latter. The flows in the connecting channels 1 and 4 are in the negative direction and those in the connecting channels 2 and 3 are in the positive direction, which are consistent with the illustrations shown in Figure 5(d). In the second phase, Chamber 1 is expanded, Chamber 2 is compressed and Chamber 3 holds still. Therefore, the chamber in the middle has the highest pressure. The flow directions in the channels are also the same as those given in Figure 5(d). In the third phase, the pressure in Chamber 3 turns out to be the highest because of

DOI: 10.1002/fld

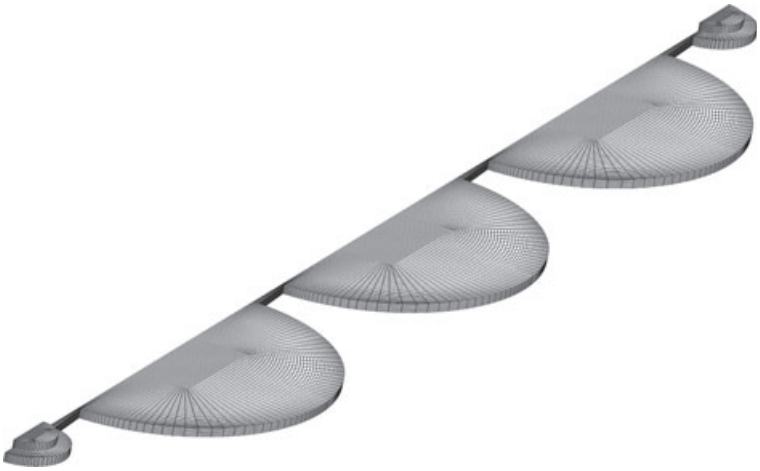

Figure 6. Computational grid for the three-chamber micropump.

compression by the membrane. By focusing on the flow in connecting channels, it can be found that the flow direction is positive in two phases and negative only in one phase. This implies that there is a net flow in the positive direction through the pump for this reversed three-phase mode operation, as will be seen next.

The variation of the flow rates predicted by the multidimensional method during one peristaltic period for the case with zero back pressure is shown in Figure 8(a) for the three-chamber pump with the three-phase mode. As indicated in the plot, $Q_{\text{in}} = Q_{\text{out}}$ throughout the entire period, $Q_{\text{c1}} = Q_{\text{c2}}$ in the first phase, $Q_{\text{c2}} = Q_{\text{out}}$ in the second phase, and $Q_{\text{c1}} = Q_{\text{in}}$ in the third phase. The above relationships represent mass conservation over the corresponding control volumes and can easily be identified from Equations (14) and (15) of the lump model. Given as an example, after summing the three equations shown in Equation (14), it is obtained that $Q_{\text{out}} - Q_{\text{in}} = Q_{\text{m1}} + Q_{\text{m2}} + Q_{\text{m3}}$. As can be seen form Equation (15), the sum $Q_{\text{m1}} + Q_{\text{m2}} + Q_{\text{m3}}$ is zero in all the three stages. The predictions by the lumped-system analysis (not shown) reveal very similar variation of the flow rate in each nozzle/diffuser channel. Figures 8(b) and (c) present those for the modes of four-phase and six-phase. In these figures, the equalities of the flow rates are identified, which can also be obtained from Equations (14) and (15).

The variation of chamber pressures is given in Figure 9. The predictions obtained using the lumped-system analysis with the assumption of steady state are also presented. Obviously, the results for the steady analysis are quite different from those obtained by the unsteady model and the CFD simulation. However, the resulting variations of the flow rates by these methods are similar. It can be seen that, as an illustration, the variation of Q_{in} shown in Figure 8(a) is roughly proportional to the pressure difference $P_{\text{in}} - P_1$ ($P_{\text{in}} = 0$) in the steady state model, which is not unexpected as implied by Bernoulli's equation. With the unsteady model, the variation of the chamber pressure lags behind the flow rate by about $\pi/2$. This phenomenon has been observed and discussed in a previous study by Tsui and Wu [24]. It can also be observed that the pressure becomes zero at the instants of phase change for the steady model because the membranes are stationary, whereas the pressure changes dramatically in the unsteady calculations. All these differences between the steady and unsteady calculations are attributed to the effect of the flow inertia.

The net flow rates for the different modes are shown in Table I. In this table, the standard three-phase mode is represented by the operating sequence shown in Figure 5(a), which was commonly used in other studies [8–14]. Both types of connecting channels are under consideration in computations. As expected, the resulting net flow rates are higher using the nozzle/diffuser because of its function of flow regulation. For understanding of the working principle of this peristaltic pump, it is better to consider the configuration with straight channels. By the lumped-system analysis, the net flow rate is negative for the standard three-phase mode and there is no net flow for the four-phase

DOI: 10.1002/fld

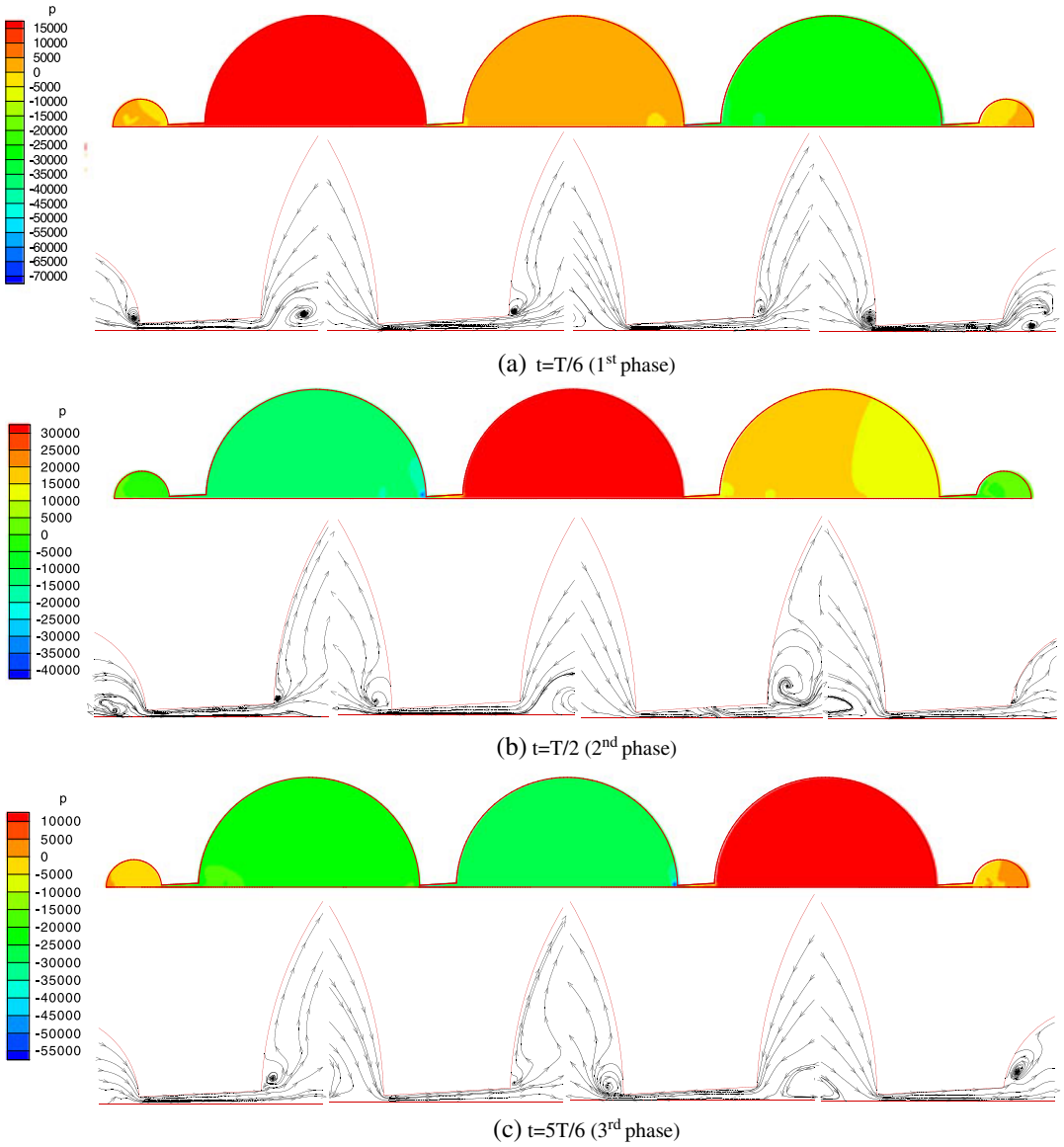

Figure 7. Pressure contours and streamlines at three stages for the three-chamber micropump operating in reversed three-phase mode with zero back pressure.

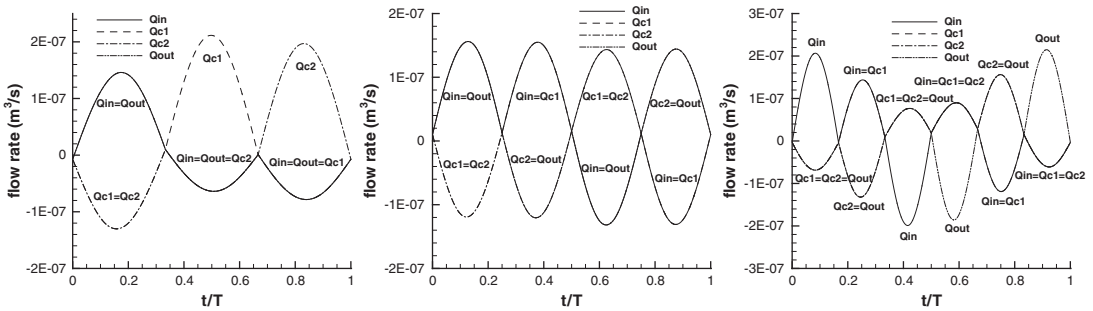

Figure 8. Variation of the flow rate predicted by multidimensional calculations.

DOI: 10.1002/fld

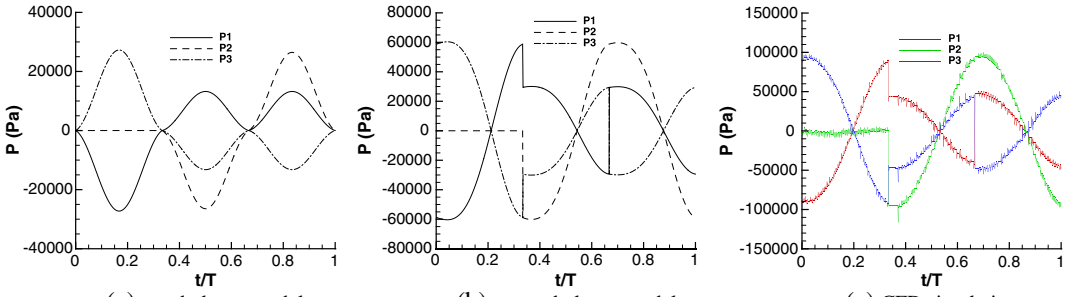

(a) steady lump model (b) unsteady lump model (c) CFD simulation

Figure 9. Variation of chamber pressure for the three-phase mode obtained by lump analyses and CFD simulation.

Table I. Net flow rates for the three-chamber peristaltic micropump (unit: ml/min).

		Standard three-phase	Four-phase	Six-phase	Reversed three-phase
Lump model	Straight channel	−0.75	0	0	0.75
	Nozzle/diffuser	0.24	1.09	1.03	1.80
CFD simulation	Straight channel	−0.56	−0.02	−0.05	0.52
	Nozzle/diffuser	0.072	0.73	0.63	1.43

and six-phase modes. It can be seen from Figure 5(a) for the three-phase mode that the flow in each connecting channel is in the direction from the inlet to the outlet in one of the three phases and the flow direction is reversed in the other two phases. Although the flow rate in the positive direction is higher than those in the negative directions, as identified in Figure 8(a), the resulting net flow is directed toward the inlet. For the even number-phase modes, Figures 5(b) and (c) indicate that the number of phases for the flow in the two directions are identical. The cancellation of the positive flow rate by the negative flow rate is revealed in Figures 8(b) and (c), leading to zero net flow for the straight channel configuration.

It is believed that the nonzero net flow rates in the CFD simulation for the even number-phase modes are caused by numerical errors, which are significant in multidimensional calculations. One source of error is due to rounding off by the computer, which becomes very serious in three-dimensional, unsteady computations and for the microscale flow systems. The other is the convergence error resulting from iterative solution methods used to solve the large systems of algebraic equations arising from the momentum and pressure-correction equations.

In view of the negative flow rate of the three-phase mode, a novel idea is to reverse the operating sequence, termed as reversed three-phase in the following, to yield positive net flow. This sequence is shown in Figure 5(d). The results are given in the last column of Table I. Obviously, the net flow rate becomes positive and has the same absolute value as that for the standard three-phase mode by the lump analysis. The performance can be further enhanced with use of the nozzle/diffuser as the connecting channel.

The results for the two-chamber configuration are presented in Table II. Similar to the three-chamber configuration, with the straight channel and the lump analysis, the net flow rate is zero for

Table II. Net flow rates for the two-chamber peristaltic micropump (unit: ml/min).

		Standard three-phase	Four-phase	Reversed three-phase
Lump model	Straight channel	−0.83	0	0.83
	Nozzle/diffuser	0.18	1.05	1.90
CFD simulation	Straight channel	−0.62	−0.013	0.63
	Nozzle/diffuser	0.056	0.69	1.52

DOI: 10.1002/fld

the four-phase mode and becomes negative for the standard three-phase mode. When the three-phase sequence is reversed, positive net flow is obtained.

Comparison of the performances at a variety of back pressures for the two-chamber and three-chamber configurations is made in Figure 10 for the reversed three-phase and four-phase modes with the nozzle/diffuser as connecting channels. Both the net flow rate and pumping efficiency are shown in the figure. The pumping efficiency is defined as

$$\eta = \frac{Q_{\text{net}}}{2m\forall_{\max}/T} \tag{16}$$

where Q_{net} represents the net flow rate, m is the number of chambers of the micropump, $2\forall_{\max}$ denotes the volume swept by the membrane, and T is the peristaltic period, being equal to $n/2f$ for the n-phase mode.

It can be seen that both the net flow rates and efficiencies are higher for the two-chamber pump than for the three-chamber pump when operating in the reversed three-phase sequence at the back pressures considered. On the contrary, the net flow rates of the three-chamber pump are greater than those of the two-chamber pump in the four-phase sequence. However, apart from the large back pressures, the efficiencies of the three-chamber pump are still lower because of the larger chamber number m. Regardless of the number of chambers, the pumping performance of the reversed-three-phase mode is superior because, as discussed above, the flow has one more phase to be in the forward direction. The performance gradually degrades when the back pressure increases. The decreasing rate for the three-chamber pump is lower, indicating that with more chambers in a pumping system its pumping performance is less sensitive to the appearance of the back pressure.

Figure 11 presents the effect of the deflection amplitude of the membrane for the three-chamber pump operating in the reversed three-phase sequence. Both the lumped-system analysis and the

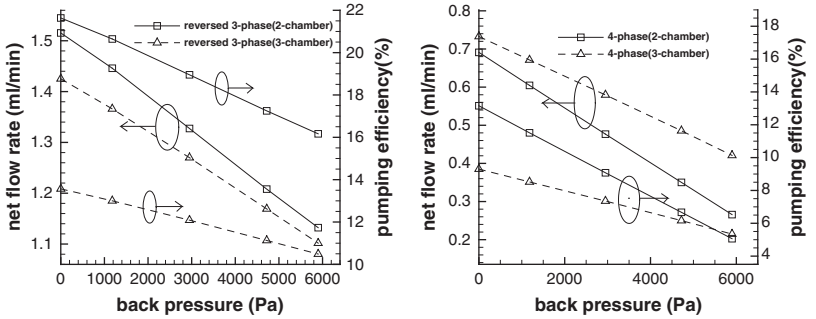

(a) reversed 3-phase (b) 4-phase

Figure 10. Net flow rates and pumping efficiencies obtained by the CFD simulation at various back pressures.

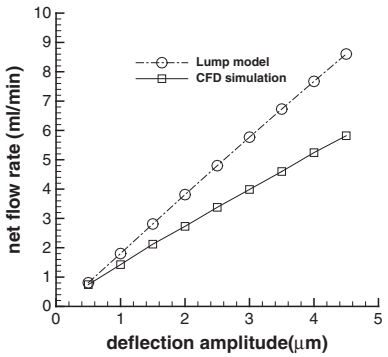

Figure 11. Net flow rates for different deflection amplitudes of the membrane operating in reversed three-phase mode.

DOI: 10.1002/fld

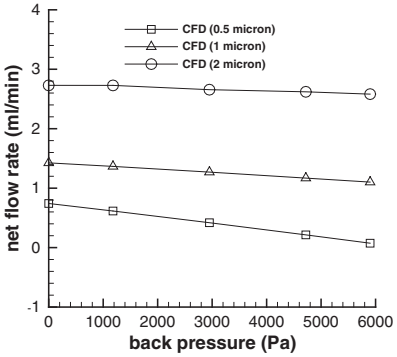

Figure 12. Net flow rates at various back pressures for three different deflection amplitudes operating in reversed three-phase mode.

CFD simulation indicate that the net flow rate increases with the amplitude. It is noted that even at the maximum value of 4.5 μm, it is still much lower than the height of the pump chamber and the compression ratio remains small. The effect of back pressure for amplitudes 0.5, 1, and 2 μm is shown in Figure 12. It can be detected that with higher amplitudes the rate decreasing with the back pressure becomes slower.

4. CONCLUSIONS

A multidimensional calculation method has been developed to analyze the performance of low-compression ratio peristaltic micropumps. The method is robust in dealing with the complicated flow situation and can portray details of the flow field. However, it is time-consuming in this analysis. It takes about 15 h of CPU time on a PC to perform one job running. Another method, based on the lumped-element concept, has also been introduced. It was shown that compared with the multidimensional simulation, the characteristics of the bulk properties such as flow rates and pressures in the pump can be properly predicted using this simple analytic method. Therefore, it is useful in the optimization or preliminary design stage of a large microfluidic system.

It can be seen from the analyses that the operational sequences of the traditional peristaltic micropump with high compression ratios are not appropriate for the low-compression pump considered in this study. For the four-phase and six-phase modes of sequence there is no net flow. The situation is worsened when the three-phase sequence is employed because the net flow rate becomes negative. The above results can easily be understood by examining the flow direction in each of the connecting channels. For the three-phase mode the flow in the backward direction happens in two phases and the flow in the forward direction only in one phase. The number of phases for the flow in the two directions are identical for the four-phase and six-phase modes. Therefore, flow regulators, such as nozzle/diffusers or valvular conduits of Tesla type, are required to rectify the flow in the even number-phase modes. A novel way to improve the pumping performance is to reverse the operational sequence of the three-phase mode such that forward flow takes place in two phases and backward flow in one phase only. It was shown that with the reversed three-phase sequence incorporating the nozzle/diffuser as the flow regulator, the pumping performance is greatly improved.

As seen in the above, the operating sequence depends upon the compression ratio of the pump. The peristaltic concepts are completely different for the compression to be extremely high or low. Therefore, it is interesting to examine its effect as the ratio value varies in between. For the analysis using CFD, the meshes in the pump chamber must be moved in accordance with the membrane vibration. As for the lumped-system analysis, the loss caused by the flow resistance in the chamber must be properly taken into account in the model.

DOI: 10.1002/fld

ACKNOWLEDGEMENTS

The long-term financial support of the National Science Council of Taiwan, R.O.C. is acknowledged.

REFERENCES

1. Oh KW, Ahn CH. A review of microvalves. *Journal of Micromechanics and Microengineering* 2006; **16**(5): R13–R39.
2. Stemme E, Stemme G. A valveless diffuser/nozzle-based fluid pump. *Sensors and Actuators A: Physical* 1993; **39**(2):159–167.
3. Gerlach T, Wurmus H. Working principle and performance of the dynamic micropump. *Sensors and Actuators A: Physical* 1995; **50**(1–2):135–140.
4. Forster FK, Bardell RL, Afromowitz MA, Sharma NR, Blanchard A. Design, fabrication and testing of fixed-valve micro-pumps. *Proceedings of the ASME Fluids Engineering Division, IMECE, FED-Vol. 234*, 1995; 39–44.
5. Anduze M, Colin S, Caen R, Camon H, Conedera V, Do Conto T. Analysis and testing of a fluidic vortex microdiode. *Journal of Micromechanics and Microengineering* 2001; **11**(2):108–112.
6. Shapiro AH, Jaffrin MY, Weinberg SL. Peristaltic pumping with long wavelengths at low Reynolds number. *Journal of Fluid Mechanics* 1969; **37**(4):799–825.
7. Fung YC, Yih CS. Peristaltic transport. *ASME Journal of Applied Mechanics* 1968; **35**:669–675.
8. Smits JG. Piezoelectric micropump with three valves working peristaltically. *Sensors and Actuators A: Physical* 1990; **21**(1–3):203–206.
9. Cao L, Mantell S, Polla D. Design and simulation of an implantable medical drug delivery system using microelectromechanical systems technology. *Sensors and Actuators A: Physical* 2001; **94**(1–2):117–125.
10. Bu M, Melvin T, Ensell G, Wilkinson JS, Evans AGR. Design and theoretical evaluation of a novel microfluidic device to be used for PCR. *Journal of Micromechanics and Microengineering* 2003; **13**(4):S125–S130.
11. Husband B, Bu M, Apostolopoulos V, Melvin T, Evans AGR. Novel actuation of an integrated peristaltic micropump. *Microelectronic Engineering* 2004; **73–74**(1):858–863.
12. Xie J, Shih J, Lin Q, Yang B, Tai Y-C. Surface micromachined electrostatically actuated micro peristaltic pump. *Lab on a Chip* 2004; **4**(5):495–501.
13. Jeong OC, Park SW, Yang SS, Pak JJ. Fabrication of a peristaltic PDMS micropump. *Sensors and Actuators A: Physical* 2005; **123–124**(2):453–458.
14. Goulpeau J, Trouchet D, Ajdari A, Tabeling P. Experimental study and modeling of polydimethylsiloxane peristaltic micropumps. *Journal of Applied Physics* 2005; **98**(4):044914–044914-9.
15. Berg JM, Anderson R, Anaya M, Lahlouh B, Holtz M, Dallas T. A two-stage discrete peristaltic micropump. *Sensors and Actuators A: Physical* 2003; **104**(1):6–10.
16. Jang L-S, Yu Y-C. Peristaltic micropump system with piezoelectric actuators. *Microsystem Technologies* 2008; **14**(2):241–248.
17. Na S, Ridgeway S, Cao L. Theoretical and experimental study of fluid behavior of a peristaltic micropump. *Proceedings of the 15th Biennial University/Government/Industry Microelectronics Symposium*, Boise, Idaho, 2003; 312–316.
18. White FM. *Fluid Mechanics*. McGraw-Hill: New York, 2008.
19. Goldschmidtboing F, Doll A, Heinrichs M, Woias P, Schrag H-J, Hopt UT. A generic analytical model for micro-diaphragm pumps with active valves. *Journal of Micromechanics and Microengineering* 2005; **15**(4):673–683.
20. Lin Q, Yang B, Xie J, Tai Y-C. Dynamic simulation of a peristaltic micropump considering coupled fluid flow and structural motion. *Journal of Micromechanics and Microengineering* 2007; **17**(2):220–228.
21. Hamrock BJ. *Fundamentals of Fluid Film Lubrication*. McGrall-Hill: New York, 1994.
22. Tsui Y-Y, Lu S-L. Evaluation of the performance of a valveless micropump by CFD and lumped-system analyses. *Sensors and Actuators A: Physical* 2008; **148**(1):138–148.
23. Ha D-H, Phan VP, Goo NS, Han CH. Three-dimensional electro-fluid-structural interaction simulation for pumping performance evaluation of a valveless micropump. *Smart Material and Structure* 2009; **18**(10):104015.
24. Tsui Y-Y, Wu S-E. Modeling of valveless micropumps. *Numerical Heat Transfer, Part A: Applications* 2009; **56**(9):727–745.
25. Patankar SV. *Numerical Heat Transfer and Fluid Flow*. McGraw-Hill: New York, 1980.
26. Issa RI. Solution of the implicitly discretised fluid flow equations by operator-splitting. *Journal of Computational Physics* 1986; **62**(1):40–65.
27. Tsui Y-Y, Pan Y-F. A pressure-correction method for incompressible flows using unstructured meshes. *Numerical Heat Transfer Part B: Fundamentals* 2006; **49**(1):43–65.
28. Kreyszig E. *Advanced Engineering Mathematics*. John Wiley & Sons: New York, 2006.

DOI: 10.1002/fld